Nano Today 35 (2020) 100984

Contents lists available at ScienceDirect

Nano Today

journal homepage: www.elsevier.com/locate/nanotoday

Colloidal crystal microneedle patch for glucose monitoring

Yi Zeng[a,b], Jinqiang Wang[a], Zejun Wang[a], Guojun Chen[a], Jicheng Yu[c], Sen Li[b], Qiwei Li[b], Hongjun Li[a], Di Wen[a], Zhongze Gu[b,*], Zhen Gu[a,*]

[a] Department of Bioengineering, University of California, Los Angeles, CA, 90095, USA
[b] State Key Laboratory of Bioelectronics, School of Biological Science and Medical Engineering, Southeast University, Nanjing, 210096, China
[c] Zenomics Inc., Los Angeles, CA, 90095, USA

ARTICLE INFO

Article history:
Received 21 August 2020
Accepted 16 September 2020

Keywords:
Diabetes
Microneedle
Glucose-responsive
Colloidal crystal
Colorimetric sensor

ABSTRACT

Blood glucose monitoring is a daily routine of people with type 1 or advanced type 2 diabetes. Efforts on minimizing invasiveness, improving portability, and enhancing sustainability of the existing glucose monitoring devices are demanding for elevating patient compliance. Here, we describe a minimally invasive colloidal crystal microneedle (MN) patch for naked-eye glucose monitoring. The glucose-responsive colloidal crystal (GCC)-MN is designed with a polymeric core to mechanically support a shell of GCC for glucose sensing and reporting. The GCC-MN patch could translate the glucose concentrations into naked-eye distinguishable color changes within 5 min, and such glucose responsiveness is reversible. Demonstrated in a type 1 diabetic mouse model, the interstitial fluid extraction, glucose sensing, and resulting glucose-relevant color display procedures are simultaneously achieved with this GCC-MN patch.
Published by Elsevier Ltd.

Introduction

Over 463 million people worldwide are currently diagnosed with diabetes mellitus, a chronic disease characterized by abnormally high blood glucose levels (BGLs) [1,2]. People with type 1 or advanced type 2 diabetes need to self-monitor their BGLs frequently to determine the time and dose of insulin injection [3]. The current electrochemical-based glucometer requires finger-prick blood sampling with consumption of numerous testing strips [4]. This invasive, painful, and costly measurement strategy often needs to be conducted multiple times each day over a life-long time, causing severe physiological and psychological burden to people with diabetes and leading to poor adherence to treatment. Therefore, a minimally invasive, painless, and economical point-of-care testing (POCT) [5] device for BGLs measurement is highly desired.

As a minimally invasive and painless alternative, microneedle (MN) patch devices have been developed and applied for extracting [6–11] and analyzing [12,13] interstitial fluid, where many molecular biomarkers are highly correlated with those in the blood [14]. Among studies of leveraging MN patch for glucose monitoring [15–18], the colorimetric MN patch system is favorable due to its visualized results without involvement of supporting equipment or complicated procedures. Nonetheless, many of these colorimetric systems contain enzymes and chromogenic substrates, which can induce concerns including enzyme denature, color quenching, by-product toxicity, and non-reusability. Colloidal crystal [19–21], a structural color material, offers a promising manner to construct a colorimetric glucose sensor comparing with the enzymatic system. By formulating colloidal crystal with a glucose-responsive material [22–25], glucose level could be reported as a structural color of colloidal crystal by manipulating the periodic structure within colloidal crystal through the glucose-responsive material. The colloidal crystal formulated colorimetric glucose sensor is enzyme-free and structural color-based, evading the issues associated with enzymatic formulations. However, the application of colloidal crystal in colorimetric MN patch is still unexplored considering the challenges in formulating sensitive glucose-responsive colloidal crystal (GCC), and assembling soft colloidal crystal with hard MN while maintaining the physical properties of colloidal crystal.

Herein, we described a GCC-MN patch for minimally invasive, painless, and naked-eye recognizable glucose colorimetric monitoring as demonstrated in a diabetic mice study. The glucose level could be displayed *in situ* as a specific structural color of the patch generated by the glucose-responsive physical nanostructure within the GCC. To convert physiological glucose levels into naked-eye recognizable structural color signals, the GCC was formulated by constructing periodic structure inside glucose-responsive fluorophenylboronic acid (FPBA) based matrix with SiO_2 nanoparticles (NPs) (Fig. 1). The GCC was coated on the surface of a

* Corresponding authors.
E-mail addresses: gu@seu.edu.cn (Z. Gu), guzhen@ucla.edu (Z. Gu).

https://doi.org/10.1016/j.nantod.2020.100984
1748-0132/Published by Elsevier Ltd.

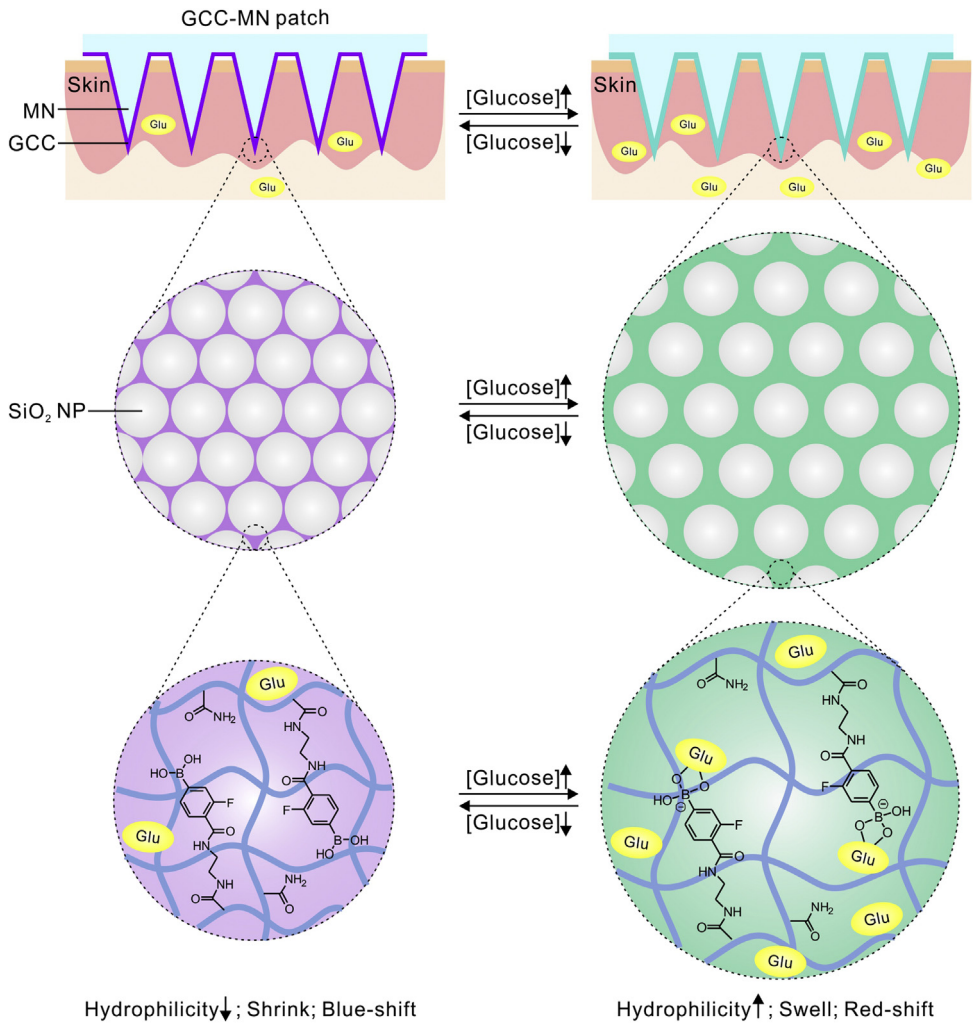

Fig. 1. Schematic illustration of the formulation of the glucose-responsive colloidal crystal modified microneedle (GCC-MN) patch, and the mechanism of the GCC-MN patch for naked-eye monitoring of glucose concentrations.

photo-polymerized MN *via* a secondary photo-crosslinking process mediated by the residual double bonds on the MN. This core-shell MN structure by assembly of the soft GCC on hard MN can not only maintain the stimulus-responsive property of the GCC, but also support sufficient mechanical strength of MN for skin penetration. Upon high glucose levels, increased glucose molecules can bind to FPBA within GCC, which increases the hydrophilicity and causes the swell of SiO_2 NPs-embedding GCC [26–28]. According to Bragg's law [29], the increased distance between periodically arranged SiO_2 NPs results in a redshift of the GCC reflection spectrum [20], displayed as a color redshift of the GCC-MN patch. Such behavior between glucose and FPBA is glucose concentration-dependent [30], yielding the GCC-MN patch with the possibility of continuous glucose monitoring. Notably, the optimized GCC formulation exhibited improved glucose responsiveness [22,23,25,31,32], manifested as the large spectral shift value (~127 nm) within physiological glucose levels, making home-based POCT feasible.

Experimental section

Materials

SiO_2 nanoparticles (~140 nm) were purchased from Nanjing Nanorainbow Biotechnology Co., Ltd (Nanjing, China). Acrylamide (≥ 99 %), poly(ethylene glycol) diacrylate (PEGDA, average Mn 700), 2-hydroxy-2-methylpropiophenone (HMPP, 97 %), dimethyl sulfoxide (DMSO, ≥ 99.9 %), glucose (≥ 99.5 %) were purchased from Sigma-Aldrich, Inc (St. Louis, USA). 4-((2-Acrylamidoethyl) carbamoyl)-3-fluorophenylboronic acid (FPBA) was synthesized by the method described in the previous study [33]. Clear resin was purchased from Formlabs Inc (Somerville, USA). Sulfo-cyanine5 NHS ester (Cy5) was purchased from Lumiprobe Corp (Maryland, USA). 1,1′-Dioctadecyl-3,3,3′,3′-tetramethylindocarbocyanine perchlorate (Dil) was obtained from Invitrogen Corp (California, USA).

Formulation of the GCC

FPBA (10.5 % w/v), acrylamide (7 % w/v), PEGDA (5 % w/w of monomers) and HMPP (5 % w/w of monomers) were dissolved in 15 % v/v SiO_2 NPs DMSO suspensions. The resulted GCC precursor solution was infused into the space between two hydrophobic glass slides where a 250 μm spacer was placed, and irradiated with 26.7 mW cm^{-2} 365 nm UV light for 20 min. After that, the photo-polymerized GCC was washed with the PBS solution until the residual DMSO in the GCC was replaced. The obtained GCC was stored in the PBS solution for further experiments.

Fabrication of the GCC-MN patch

Clear resin was filled into an MN (pyramidal, 400 μm in width, 900 μm in height, 800 μm tip-tip spacing) patch mold under vacuum and was polymerized under UV light (26.7 mW cm^{-2}, 365 nm) for 5 min. To increase the mechanical strength, the photopolymerized MN patch was further cured under 405 nm light (1.25 mW cm^{-2}) for 25 min, and then was detached from the mold. The as-prepared GCC precursor solution was infused into the previously used MN patch mold. Before inserting the cured MN patch into the GCC solution-containing mold, a 250 μm spacer was placed between the MN patch and the mold to control the coating thickness. Afterward, the GCC precursor solution-containing mold with the cured MN patch was irradiated with 365 nm UV light (26.7 mW cm^{-2}) for 15 min. Finally, the GCC-MN patch was detached from the mold, washed, and stored in the PBS solution.

In vitro *glucose monitoring*

To study the glucose responsiveness of the GCC, the GCC or the GCC-MN patch (5 × 5 array) was immersed in 10 mL glucose-containing PBS solution and observed at different incubation time points.

In vivo *glucose monitoring*

To evaluate the *in vivo* glucose responsiveness of the GCC-MN patch, diabetic mice (C57BL/6J, Jackson Lab) and normal mice (C57BL/6J, Jackson Lab) were used as the hyperglycemic model and the normoglycemic control, respectively. All animal studies complied with the protocol (ARC # 2018-062) approved by the Institutional Animal Care and Use Committee at the University of California, Los Angeles (UCLA). To perform glucose monitoring with the GCC-MN patch, the mice were shaved and anesthetized before the experiment. The BGLs of the mice were measured with an Accu-Chek Aviva® meter (Roche Diabetes Care, Inc.) before the GCC-MN patch insertion. Then, the GCC-MN patch was pressed on the skin of the mouse for 10 s and retained for a specific time. Thereafter, the GCC-MN patch was removed from the skin and the color change of the GCC-MN patch was recorded with a camera.

Characterizations

The reflection spectra were recorded with a spectrometer (OCEAN-HDX-XR, Ocean Insight, USA). The SEM images were obtained with a field emission scanning electron microscope (Supra® 40VP, Zeiss, Germany). The 3D fluorescence images were obtained and reconstructed with a confocal microscope (Leica TCS-SP8, Leica Microsystems, Germany) and Imaris software, respectively. The mechanical strength tests were conducted by using the compression mode of Instron 5560 (Instron Corporation, Norwood, Mass). ^{1}H nuclear magnetic resonance spectrum was tested with Bruker AV400 broadband FT NMR spectrometer (Bruker, Massachusetts, USA). The averaged hue values were calculated with Adobe Photoshop CC 2017 software.

Results and discussion

The structural color of colloidal crystal is dominated by its periodic structure according to Bragg's law:

$$\lambda = 1.633 d n_{avg} \quad (1)$$

where λ represents the reflection peak wavelength, d is the interplanar distance, and n_{avg} is the averaged refractive index [34]. Thus the color of colloidal crystal could be manipulated by adjusting the distance d between SiO_2 NPs (~140 nm diameter, Fig. 2a) through changing the concentration of SiO_2 NPs (Fig. 2b). In preparing the GCC, the concentration of SiO_2 NPs was set to 15 % v/v to ensure the color of the GCC was in the visible region under the physiological glucose concentrations. Glucose-responsive FPBA (10.5 % w/v) and acrylamide (7 % w/v) were incorporated to construct a glucose-responsive hydrogel network of the GCC. The formulated GCC was colorless since the short distance between the orderly packed SiO_2 NPs drove the photonic band gap of the GCC into the invisible UV range (Fig. 2c).

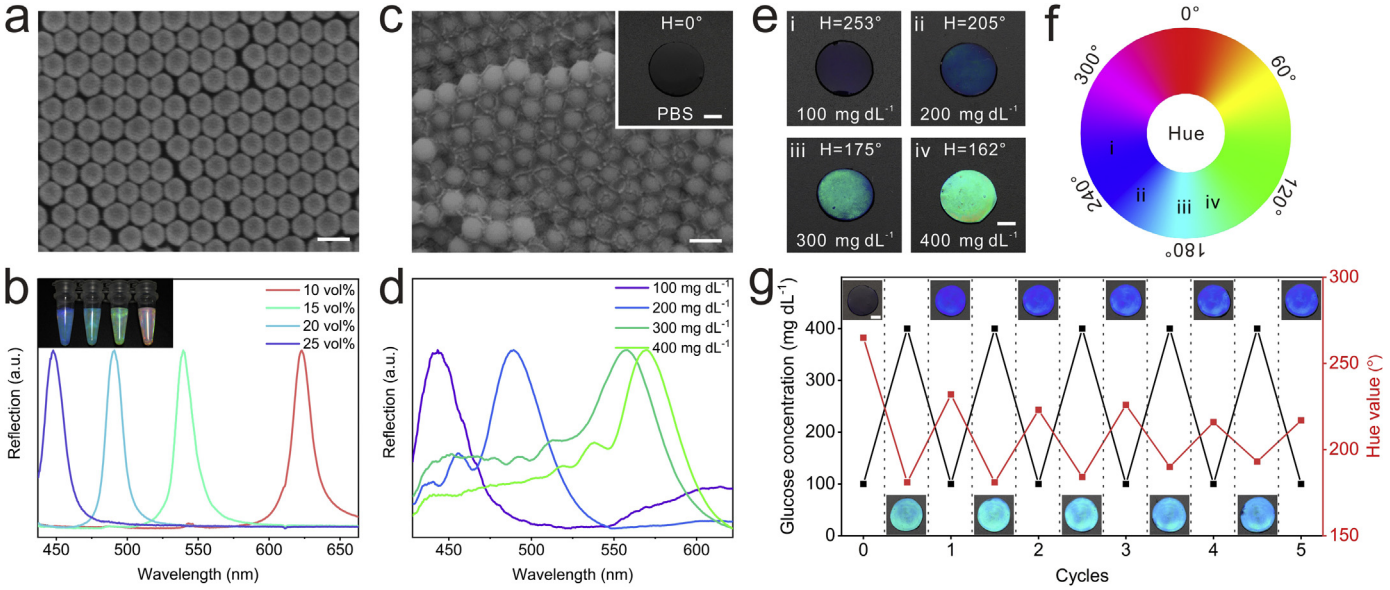

Fig. 2. Characterizations of the GCC. a) The SEM image of SiO_2 NPs (~140 nm). Scale bar: 200 nm. b) The normalized reflection spectra and the digital photograph of SiO_2 NPs dispersed solutions. c) The SEM image and optical photo of the GCC. Scale bars: 200 nm and 2 mm. d) The normalized reflection spectra of the GCC after treated with the indicated concentrations of the glucose solutions for 20 min. e) The corresponding digital images of the GCC in d). Scale bar: 2 mm. H represents the averaged hue value of the GCC. f) The picture of a hue circle where the images in e) are marked at the corresponding positions. g) The reversibility of the GCC after treated with different glucose solutions. The GCC was immersed in 100 and 400 mg dL^{-1} glucose solutions for 20 min alternately. Scale bar: 2 mm.

The color and the structure of the GCC changed while immersed into various concentrations of glucose solutions (100, 200, 300, and 400 mg dL^{-1}). The reflection peak of the GCC red-shifted with the prolonged reaction time and increased glucose concentration (**Fig. S1**). Here, the reaction time was set to 20 min for the following characterizations to achieve distinct color discrimination of the GCC under different glucose concentrations. The reflection peak of the GCC shifted from 443 nm to 570 nm (127 nm spectral shift) when the glucose concentration was increased from 100 to 400 mg dL^{-1} (Fig. 2d), demonstrating the excellent glucose responsiveness and the feasibility of the GCC as a naked-eye recognizable colorimetric glucose sensor. The GCC exhibited specific colors under different glucose concentrations, specifically the color of the GCC changed from violet (100 mg dL^{-1} glucose) to blue (200 mg dL^{-1} glucose), and further to green (400 mg dL^{-1} glucose) by increasing glucose concentrations (Fig. 2e).

To quantify the color of the GCC, averaged hue value (H) [35], the color appearance parameter, of the GCC under different glucose concentrations was measured and presented in a hue circle (Fig. 2e and f). The averaged hue values of the GCC decreased with increased glucose concentrations, owing to the redshift of GCC color in response to elevated glucose concentrations. Upon high glucose concentrations, increased glucose molecules bind to FPBA, enhancing the hydrophilicity of the GCC and causing the GCC to swell. This is supported by the SEM images, which depicted the enlarged particle distance and expanded hydrogel network (**Fig. S2**). The binding of glucose to FPBA is reversible [30], thus the FPBA based formulation shows reversible glucose responsiveness. The GCC was put in 100 mg dL^{-1} and 400 mg dL^{-1} glucose solutions alternately, during which the color and averaged hue value of the GCC displayed reversible changes even after five cycles (Fig. 2g). The reversible glucose responsiveness endows the GCC with the potential of continuous glucose monitoring and recyclability (**Fig. S3**).

To assemble the soft GCC with hard MN while maintaining both of the glucose responsiveness of the GCC and the ability of MN to puncture the skin, the GCC was secondarily modified on the surface of MN through photo-crosslinking. As illustrated in Fig. 3a, the resin was infused into an MN mold and photo-crosslinked by UV

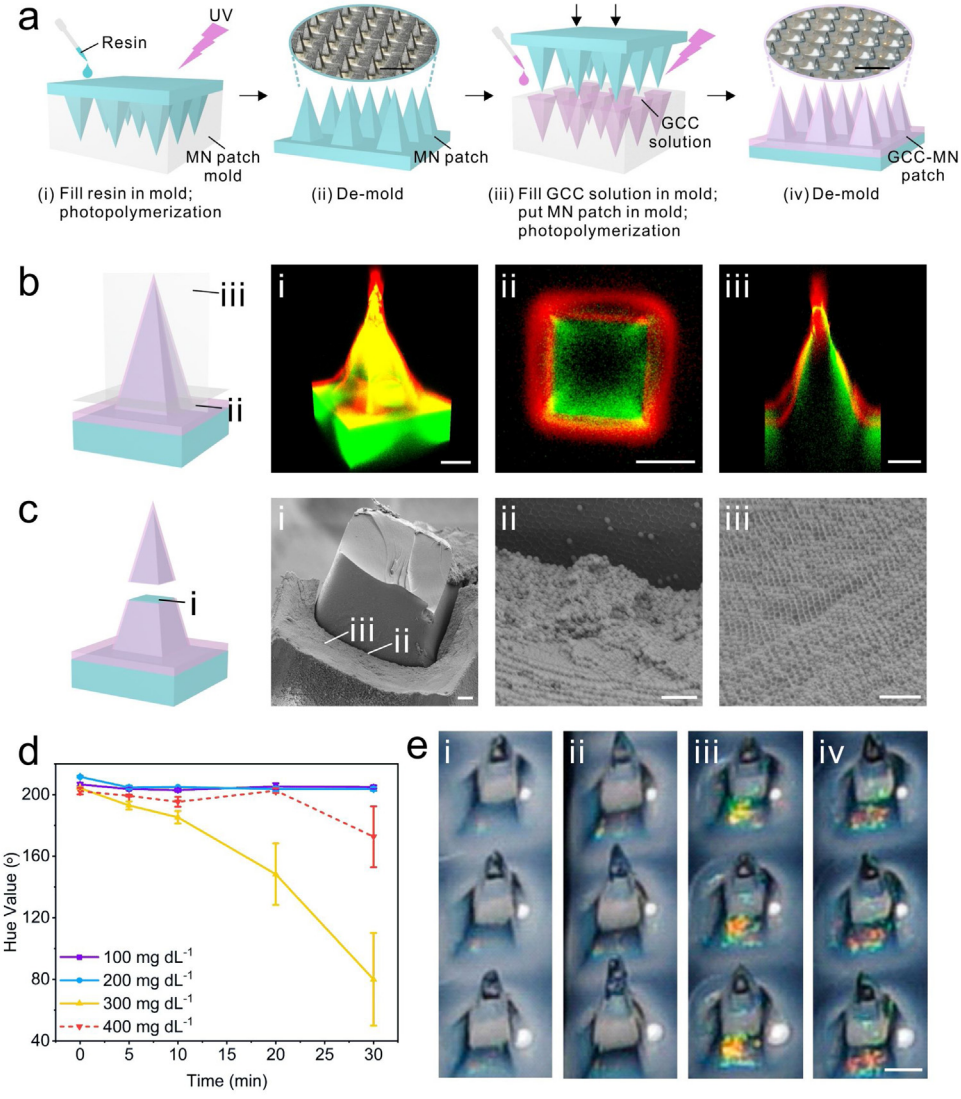

Fig. 3. Characterizations of the GCC-MN patch. a) The schematic of the fabrication process of the GCC-MN patch. The insets are the photographs of bare MN patch and the GCC-MN patch, respectively. Scale bars: 1 mm. b) Confocal microscopy images of the GCC-MN. i) The three-dimensional reconstructed confocal image. ii-iii) The cross-sectional confocal images. Scale bars: 200 μm. c) The SEM images of the GCC-MN. i) The cross-sectional SEM image of the GCC-MN. ii-iii) The magnified views of i). Scale bars: 1 μm. d) The averaged hue value of the GCC-MN after treated with different glucose solutions (100, 200, 300, and 400 mg dL^{-1}) for a different time. The data are presented as mean ± SD (n = 3). e) The digital images of the GCC-MN treated with i) 100, ii) 200, iii) 300, and iv) 400 mg dL^{-1} glucose solutions for 30 min, respectively. Scale bar: 200 μm.

light. The cured MN patch was then put into an MN mold containing GCC precursor solution and photo-crosslinked by UV light for the second time. In that way, the GCC was coated on the surface of the MN by cross-linking with the residual double bonds on the MN (**Fig. S4**). Confocal microscopy and scanning electron microscopy (SEM) were leveraged to evaluate the morphology of the GCC-MN. As shown in the three-dimensional reconstructed confocal images, distinguished boundary and close contact between Cy5-labeled GCC and Dil-labeled MN were identified (Fig. 3b), confirming the GCC was coated on the MN. Furthermore, the periodic structure within the GCC, which is the guarantee of the colorimetric feasibility of the GCC-MN, was investigated. The GCC-MN was cut off from the middle and the cross-section was observed with SEM. The residual hydrogel network was firmly attached to the exterior of the MN, and the SiO_2 NPs within GCC were orderly packed in the hydrogel networks, which was similar to that of the GCC (Fig. 3c).

The *in vitro* glucose responsiveness of the GCC-MN patch was evaluated by exposing the core-shell MN patches into different glucose solutions (100, 200, 300, and 400 mg dL^{-1}) for various periods (0, 5, 10, 20, and 30 min). Their averaged hue values were subsequently calculated (**Fig. S5** and Fig. 3d). The hue value of the GCC-MN did not change significantly when the glucose concentration was below 200 mg dL^{-1}. When the glucose concentration was increased to 300 mg dL^{-1}, an obvious green color accompanied by a dramatic drop in hue value was identified within 5 min (**Fig. S5**). As the immersion time increased, the color of the GCC-MN further redshifted to yellow and the hue value dropped over a period of 30 min. A similar redshift was also observed for the GCC-MN when it was exposed to a 400 mg dL^{-1} glucose solution where the color of the GCC-MN redshifted to red in 30 min. It is worth mentioning that the averaged hue value of the GCC-MN under 400 mg dL^{-1} glucose concentration (red dash line in Fig. 3d) did not drop as expected. This is due to the interference caused by the hue value of red (0° or 360°) to the averaged hue value calculation. The color redshift trend of the GCC-MN in response to the elevated glucose concentrations (Fig. 3e) was similar to that of the GCC alone. The slight color difference between the GCC-MN and the GCC alone under a specific glucose concentration might be attributed to the experimental variables caused by the different fabrication processes. Collectively, the formulated GCC-MN patch could change color in a glucose-responsive manner, especially when the glucose concentration was over 200 mg dL^{-1}, the condition that mouse is considered to be hyperglycemic.

The secondary modification design integrated the gel-like GCC with the skin-penetrating MN scaffold, allowing the minimally invasive *in vivo* study (Fig. 4a) with soft materials. The GCC-MN showed a similar mechanical property with the unmodified MN, and no fracture (force) was observed during the test, demonstrating that the hardness and toughness of the MN were well maintained after the GCC coating (Fig. 4b). The GCC-MN patch was further inserted into the mouse skin which was subsequently stained by trypan blue, confirming the insertion capability of the GCC-MN (Fig. 4b). The *in vivo* glucose monitoring study with the GCC-MN patch was performed on both streptozotocin (STZ)-induced C57BL/6J diabetic mice and healthy C57BL/6J mice, which served as the hyperglycemic model and the normoglycemic control, respectively. Five min after the GCC-MN patch application, the patches were removed and analyzed. The GCC-MN remained colorless in the control group, while the GCC-MN used in the hyperglycemic group displayed a green color (Fig. 4c). Considering the interaction

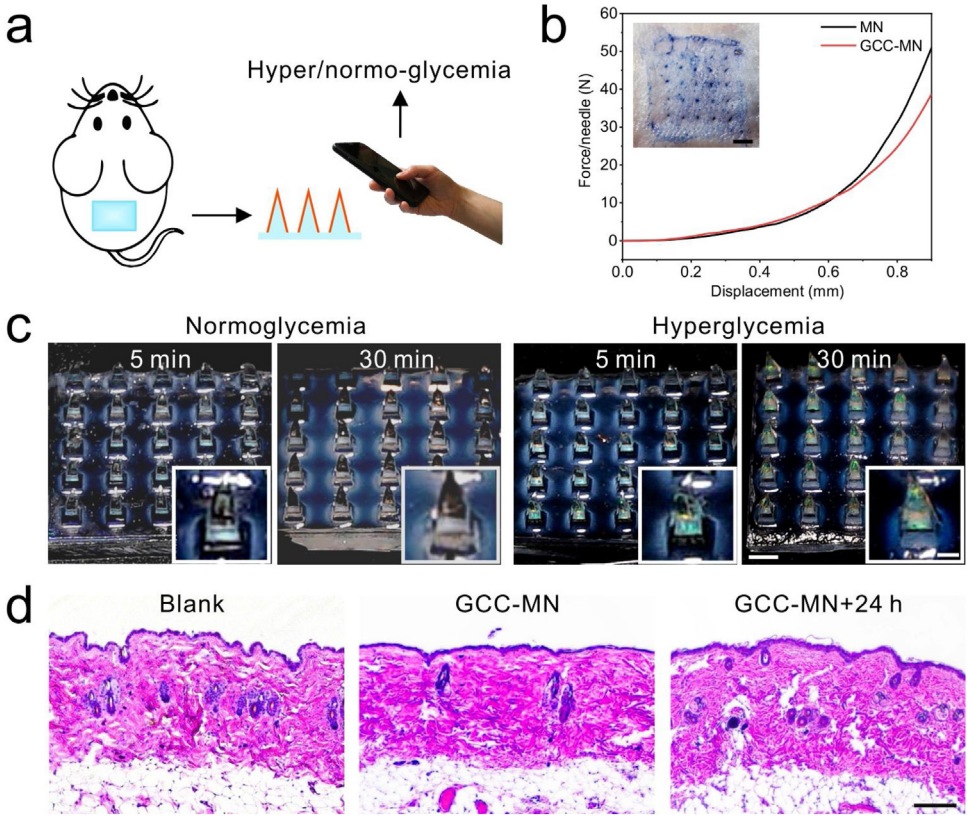

Fig. 4. The *in vivo* studies of the GCC-MN patch. a) The schematic of *in vivo* monitoring glucose levels with the GCC-MN patch. The hyperglycemia or normoglycemia could be identified with eyes or camera according to the color change of the GCC-MN. b) Mechanical characterizations of the GCC-MN and bare MN. The inset is the trypan blue stained mouse skin after applied with the GCC-MN patch. Scale bar: 1 mm. c) The digital photos of the GCC-MN patches after inserting normoglycemic (~180 mg dL^{-1} glucose) or hyperglycemic (~400 mg dL^{-1} glucose) mice skins for a different time. Scale bars: 500 μm, 200 μm (the inset). d) H&E staining pictures of untreated mouse skin, mouse skin after applied with the GCC-MN patch, and mouse skin one day after GCC-MN patch treatment, respectively. The GCC-MN patch treatment time is 30 min. Scale bar: 100 μm.

between the GCC-MN and interstitial fluid is time-dependent, the application time of the GCC-MN patch on the mouse was further prolonged to 30 min. A significantly distinguished color change was observed for the GCC-MN in the hyperglycemic group, while the GCC-MN applied to the normal mouse remained colorless (Fig. 4c), demonstrating the feasibility of GCC-MN patch for hyperglycemia monitoring in the diabetic mouse. Of note, the GCC-MN patch is enzyme-free and dye-free, eliminating the associated biocompatibility issues. Hematoxylin and eosin (H&E) staining of the mouse skins obtained from the treated sites of the GCC-MN was performed. The skin showed negligible inflammation after GCC-MN insertion as compared to the untreated skin, proving biosafety of our GCC-MN patch (Fig. 4d).

Conclusions

In conclusion, we have developed a colloidal crystal MN patch for minimally invasive, painless, and naked-eye recognizable glucose colorimetric monitoring. The GCC showed improved glucose sensitivity, rendering naked-eye glucose monitoring feasible. The secondary modification strategy integrated the GCC with MN, which enabled the *in vivo* glucose colorimetric monitoring with naked eyes in an enzyme-free way. As demonstrated in a diabetic mouse model, the GCC-MN patch was qualified to *in situ* detect hyperglycemia in mice without significant inflammation concern. With this simple and versatile secondary modification method, MN patch could be tailored with theranostic functions for broad applications beyond glucose monitoring in drug delivery and POCT fields [36–38].

CRediT authorship contribution statement

Yi Zeng: Conceptualization, Methodology, Validation, Writing - original draft. **Jinqiang Wang:** Methodology, Investigation, Writing - original draft. **Zejun Wang:** Investigation, Writing - original draft. **Guojun Chen:** Investigation, Writing - original draft. **Jicheng Yu:** Methodology, Investigation. **Sen Li:** Methodology, Investigation. **Qiwei Li:** Methodology, Investigation. **Hongjun Li:** Investigation, Formal analysis. **Di Wen:** Investigation. **Zhongze Gu:** Conceptualization, Methodology, Writing - review & editing. **Zhen Gu:** Conceptualization, Methodology, Writing - review & editing, Funding acquisition.

Declaration of Competing Interest

The authors reported no declarations of interest.

Acknowledgments

This work was supported by the grants from National Science Foundation (grant no. 1708620), and American Diabetes Association (grant no. 1-15-ACE-21).

Appendix A. Supplementary data

Supplementary data associated with this article can be found, in the online version, at https://doi.org/10.1016/j.nantod.2020.100984.

References

[1] American Diabetes Association, Introduction: standards of medical care in diabetes—2019, Diabetes Care 42 (2019) S1–S2, http://dx.doi.org/10.2337/dc19-sint01.
[2] International Diabetes Federation, Diabetes Facts & Figures, 2020 (Accessed 5 May 2020) https://www.idf.org/aboutdiabetes/what-is-diabetes/facts-figures.html.
[3] E.W. Gregg, N. Sattar, M.K. Ali, The changing face of diabetes complications, Lancet Diabetes Endocrinol. 4 (2016) 537–547, http://dx.doi.org/10.1016/S2213-8587(16)30010-9.
[4] L. Czupryniak, L. Barkai, S. Bolgarska, A. Bronisz, J. Broz, K. Cypryk, M. Honka, A. Janez, M. Krnic, N. Lalic, E. Martinka, D. Rahelic, G. Roman, T. Tankova, T. Várkonyi, B. Wolnik, N. Zherdova, Self-monitoring of blood glucose in diabetes: from evidence to clinical reality in central and eastern europe - Recommendations from the international central-eastern european expert group, Diabetes Technol. Ther. 16 (2014) 460–475, http://dx.doi.org/10.1089/dia.2013.0302.
[5] V. Gubala, L.F. Harris, A.J. Ricco, M.X. Tan, D.E. Williams, Point of care diagnostics: status and future, Anal. Chem. 84 (2012) 487–515, http://dx.doi.org/10.1021/ac2030199.
[6] P. Xue, L. Zhang, Z. Xu, J. Yan, Z. Gu, Y. Kang, Blood sampling using microneedles as a minimally invasive platform for biomedical diagnostics, Appl. Mater. Today 13 (2018) 144–157, http://dx.doi.org/10.1016/j.apmt.2018.08.013.
[7] J. Wang, Z. Wang, J. Yu, A.R. Kahkoska, J.B. Buse, Z. Gu, Glucose-responsive insulin and delivery systems: innovation and translation, Adv. Mater. 32 (2020), 1902004, http://dx.doi.org/10.1002/adma.201902004.
[8] X. Zhang, G. Chen, F. Bian, L. Cai, Y. Zhao, Encoded microneedle arrays for detection of skin interstitial fluid biomarkers, Adv. Mater. 31 (2019), 1902825, http://dx.doi.org/10.1002/adma.201902825.
[9] R. Paul, A.C. Saville, J.C. Hansel, Y. Ye, C. Ball, A. Williams, X. Chang, G. Chen, Z. Gu, J.B. Ristaino, Q. Wei, Extraction of plant DNA by Microneedle Patch for rapid detection of plant diseases, ACS Nano 13 (2019) 6540–6549, http://dx.doi.org/10.1021/acsnano.9b00193.
[10] D. Al Sulaiman, J.Y.H. Chang, N.R. Bennett, H. Topouzi, C.A. Higgins, D.J. Irvine, S. Ladame, Hydrogel-coated microneedle arrays for minimally invasive sampling and sensing of specific circulating nucleic acids from skin interstitial fluid, ACS Nano 13 (2019) 9620–9628, http://dx.doi.org/10.1021/acsnano.9b04783.
[11] H. Chang, M. Zheng, X. Yu, A. Than, R.Z. Seeni, R. Kang, J. Tian, D.P. Khanh, L. Liu, P. Chen, C. Xu, A swellable microneedle patch to rapidly extract skin interstitial fluid for timely metabolic analysis, Adv. Mater. 29 (2017), 1702243, http://dx.doi.org/10.1002/adma.201702243.
[12] A.M.V. Mohan, J.R. Windmiller, R.K. Mishra, J. Wang, Continuous minimally-invasive alcohol monitoring using microneedle sensor arrays, Biosens. Bioelectron. 91 (2017) 574–579, http://dx.doi.org/10.1016/j.bios.2017.01.016.
[13] Q. Jin, H.-J. Chen, X. Li, X. Huang, Q. Wu, G. He, T. Hang, C. Yang, Z. Jiang, E. Li, A. Zhang, Z. Lin, F. Liu, X. Xie, Reduced graphene oxide nanohybrid-assembled microneedles as mini-invasive electrodes for real-time transdermal biosensing, Small 15 (2019), 1804298, http://dx.doi.org/10.1002/smll.201804298.
[14] S.R. Corrie, J.W. Coffey, J. Islam, K.A. Markey, M.A.F. Kendall, Blood, sweat, and tears: developing clinically relevant protein biosensors for integrated body fluid analysis, Analyst 140 (2015) 4350–4364, http://dx.doi.org/10.1039/c5an00464k.
[15] K.B. Kim, W.C. Lee, C.-H. Cho, D.-S. Park, S.J. Cho, Y.-B. Shim, Continuous glucose monitoring using a microneedle array sensor coupled with a wireless signal transmitter, Sens. Actuators, B Chem. 281 (2019) 14–21, http://dx.doi.org/10.1016/j.snb.2018.10.081.
[16] D. Nicholas, K.A. Logan, Y. Sheng, J. Gao, S. Farrell, D. Dixon, B. Callan, A.P. McHale, J.F. Callan, Rapid paper based colorimetric detection of glucose using a hollow microneedle device, Int. J. Pharm. 547 (2018) 244–249, http://dx.doi.org/10.1016/j.ijpharm.2018.06.002.
[17] Z. Wang, H. Li, J. Wang, Z. Chen, G. Chen, D. Wen, A. Chan, Z. Gu, Transdermal colorimetric patch for hyperglycemia sensing in diabetic mice, Biomaterials 237 (2020), 119782, http://dx.doi.org/10.1016/j.biomaterials.2020.119782.
[18] H. Lee, T.K. Choi, Y.B. Lee, H.R. Cho, R. Ghaffari, L. Wang, H.J. Choi, T.D. Chung, N. Lu, T. Hyeon, S.H. Choi, D.-H. Kim, A graphene-based electrochemical device with thermoresponsive microneedles for diabetes monitoring and therapy, Nat. Nanotechnol. 11 (2016) 566–572, http://dx.doi.org/10.1038/nnano.2016.38.
[19] J.H. Holtz, S.A. Asher, Polymerized colloidal crystal hydrogel films as intelligent chemical sensing materials, Nature 389 (1997) 829–832.
[20] Y. Zhao, L. Shang, Y. Cheng, Z. Gu, Spherical colloidal photonic crystals, Acc. Chem. Res. 47 (2014) 3632–3642, http://dx.doi.org/10.1021/ar500317s.
[21] Y. Zhao, Z. Xie, H. Gu, C. Zhu, Z. Gu, Bio-inspired variable structural color materials, Chem. Soc. Rev. 41 (2012) 3297–3317, http://dx.doi.org/10.1039/c2cs15267c.
[22] S.A. Asher, V.L. Alexeev, A.V. Goponenko, A.C. Sharma, I.K. Lednev, C.S. Wilcox, D.N. Finegold, Photonic crystal carbohydrate sensors: low ionic strength sugar sensing, J. Am. Chem. Soc. 125 (2003) 3322–3329, http://dx.doi.org/10.1021/ja021037h.
[23] D. Nakayama, Y. Takeoka, M. Watanabe, K. Kataoka, Simple and precise preparation of a porous gel for a colorimetric glucose sensor by a templating technique, Angew. Chem. Int. Ed. 42 (2003) 4197–4200, http://dx.doi.org/10.1002/anie.200351746.
[24] V.L. Alexeev, S. Das, D.N. Finegold, S.A. Asher, Photonic crystal glucose-sensing material for noninvasive monitoring of glucose in tear fluid, Clin. Chem. 50 (2004) 2353–2360, http://dx.doi.org/10.1373/clinchem.2004.039701.
[25] F. Xue, Z. Meng, F. Wang, Q. Wang, M. Xue, Z. Xu, A 2-D photonic crystal hydrogel for selective sensing of glucose, J. Mater. Chem. A 2 (2014) 9559–9565, http://dx.doi.org/10.1039/c4ta01031k.

[26] A. Kikuchi, K. Suzuki, O. Okabayashi, H. Hoshino, K. Kataoka, Y. Sakurai, T. Okano, Glucose-sensing electrode coated with polymer complex gel containing phenylboronic acid, Anal. Chem. 68 (1996) 823–828, http://dx.doi.org/10.1021/ac950748d.
[27] A. Matsumoto, S. Ikeda, A. Harada, K. Kataoka, Glucose-responsive polymer bearing a novel phenylborate derivative as a glucose-sensing moiety operating at physiological pH conditions, Biomacromolecules 4 (2003) 1410–1416, http://dx.doi.org/10.1021/bm034139o.
[28] Y.-J. Lee, S.A. Pruzinsky, P.V. Braun, Glucose-sensitive inverse opal hydrogels: analysis of optical diffraction response, Langmuir 20 (2004) 3096–3106, http://dx.doi.org/10.1021/la035555x.
[29] W.H. Bragg, W.L. Bragg, The reflexion of X-rays by crystals, Proc. R. Soc. A 88 (1913) 428–438.
[30] S.D. Bull, M.G. Davidson, J.M.H. Van Den Elsen, J.S. Fossey, A.T.A. Jenkins, Y.-B. Jiang, Y. Kubo, F. Marken, K. Sakurai, J. Zhao, T.D. James, Exploiting the reversible covalent bonding of boronic acids: recognition, sensing, and assembly, Acc. Chem. Res. 46 (2013) 312–326, http://dx.doi.org/10.1021/ar300130w.
[31] M. Elsherif, M.U. Hassan, A.K. Yetisen, H. Butt, Wearable contact Lens biosensors for continuous glucose monitoring using smartphones, ACS Nano 12 (2018) 5452–5462, http://dx.doi.org/10.1021/acsnano.8b00829.
[32] X. Hong, Y. Peng, J. Bai, B. Ning, Y. Liu, Z. Zhou, Z. Gao, A novel opal closest-packing photonic crystal for naked-eye glucose detection, Small 10 (2014) 1308–1313, http://dx.doi.org/10.1002/smll.201302788.
[33] A. Matsumoto, T. Ishii, J. Nishida, H. Matsumoto, K. Kataoka, Y. Miyahara, A synthetic approach toward a self-regulated insulin delivery system, Angew. Chem. Int. Ed. 51 (2012) 2124–2128, http://dx.doi.org/10.1002/anie.201106252.
[34] Y. Zhao, Z. Xie, H. Gu, L. Jin, X. Zhao, B. Wang, Z. Gu, Multifunctional photonic crystal barcodes from microfluidics, NPG Asia Mater. 4 (2012) 1–7, http://dx.doi.org/10.1038/am.2012.46.
[35] M.D. Fairchild, Color appearance models : CIECAM02 and beyond, Tutor. Notes, IS&T/SID 12th Color Imaging Conf (2004).
[36] Y. Lu, A.A. Aimetti, R. Langer, Z. Gu, Bioresponsive materials, Nat. Rev. Mater. 2 (2016) 1–17, http://dx.doi.org/10.1038/natrevmats.2016.75.
[37] K.J. Lee, M.J. Goudie, P. Tebon, W. Sun, Z. Luo, J. Lee, S. Zhang, K. Fetah, H.-J. Kim, Y. Xue, M.A. Darabi, S. Ahadian, E. Sarikhani, W. Ryu, Z. Gu, P.S. Weiss, M.R. Dokmeci, N. Ashammakhi, A. Khademhosseini, Non-transdermal microneedles for advanced drug delivery, Adv. Drug Deliv. Rev. (2019), http://dx.doi.org/10.1016/j.addr.2019.11.010.
[38] J. Yu, Y. Zhang, J. Yan, A.R. Kahkoska, Z. Gu, Advances in bioresponsive closed-loop drug delivery systems, Int. J. Pharm. 544 (2018) 350–357, http://dx.doi.org/10.1016/j.ijpharm.2017.11.064.